A R C H I V E S O F M E T A L L U R G Y A N D M A T E R I A L S
Volume 51 2006 Issue 3

E. FRAŚ*, M. GÓRNY*, H. LOPEZ**

THIN WALL DUCTILE IRON CASTINGS AS A GRADIENT MATERIAL

CIENKOŚCIENNE ODLEWY Z ŻELIWA SFEROIDALNEGO JAKO MATERIAŁ GRADIENTOWY

In this paper a theoretical structural analysis of super thin walled casting made of ductile iron is presented. Analysis shows that such castings have inhomogenius gradient structure, manifested by different: number of graphite nodules and ferritte and cementite fraction as a result of altered cooling rate along casting length. Critical distance above which the chills will be presents and graditent of graphite nodule count is inteoduced. Theoretical investigations were experimentally verified for a casting with 1.6 mm wall thickness where graphite nodule count N, ferrite f_f and cementite eutectic f_c fraction and gradients G_N, G_{f_f}, G_{f_c} as a function of distance from runner were estimated. Finally rather a good agreement was found between the theoretical predictions and the experimental outcome.

W pracy przedstawiono teoretyczną analizę strukturalną super cieńkościennych odlewów z żeliwa sferoidalnego. Analiza wykazuje, że takie odlewy mają niejednorodną strukturę gradientową, przejawiającą się: różną liczbą kulek grafitu, udziałem ferrytu oraz eutektyki cementytowej jako efekt zmiennej szybkości stygnięcia. W pracy przedstawiono wyrażenie na krytyczną odległość, powyżej której występują zabielenia w odlewie oraz gradient liczby kulek grafitu. Badania teoretyczna zostały zweryfikowane dla odlewu o grubośći ścianki 1.6 mm gdzie określono liczbę kulek grafitu, udział ferrytu f_f i cementytu f_c oraz gradienty G_N, G_{f_f}, G_{f_c} w funkcji odległości od belki wlewowej. Wykazano, że przedstawiona teoria dobrze opisuje wyniki eksperymentalne.

1. Introduction

Advanced construction application requiare multifunctional working elements having more then one custom properties. As a result new matrials were developed which are called Functionally Gradient Materials (FGM) [1–3]. To such type of materials ductile iron can be credited which characterize high sensitivity on cooling rate what in consequence leads to structural gradients G_x that is constant changes of structural features of cast iron (properties accordingly) along one of it direction. In general, in recent years there has been an increasing demand for thin-wall ductile iron castings with wall thickness below 3 mm (TWDI) with high strength-weight ratios [4, 5].

In TWDI, there are numerous studies on the solidification morphologies [6], microstructural charactherization [7, 8], mechanical properties [9–14], carbide formation factors [15, 16], production [17, 18]], solid state transformations [19, 21] and mold filling [21]. Moreover, according to the literature, there are different experimental relationships between the chemical composition [7, 15, 18, 19], pouring temperature [15], spheroidization and inoculation practice [15, 17, 22], casting geometry [11], plate thickness [7, 15, 21], mold material and nodule count [23], critical nodule count and critical plate thickness below which the chills develops (see Fig. 1).

These experimental relationships are very useful but they are limited in their physical meaning and in describing the mechanisms involved during the chill development of cast iron and the nodule formation. Hence, it can be said that the experimental relationships reported in the literature are just a type of "black box" which is fed on one side with the casting input parameters and the resultant solidification microstructure on the other side of the box, as shown schematically in Fig. 1. Accordingly, in this work an attempt is made to elucidate "what happens" in this black box by considering the solidification process of cast iron. In particular, in this work analytical expressions are derived for explanation of formation mechanism of primary gradient structure of TWDI castings.

* AGH – UNIVERSITY OF SCIENCE AND TECHNOLOGY, 30-059 KRAKÓW, 23 REYMONTA STR., POLAND
** UNIVERSITY OF WISCONSIN-MILWAUKEE, 3200N. CRAMER, MILWAUKEE, WI 53201, USA

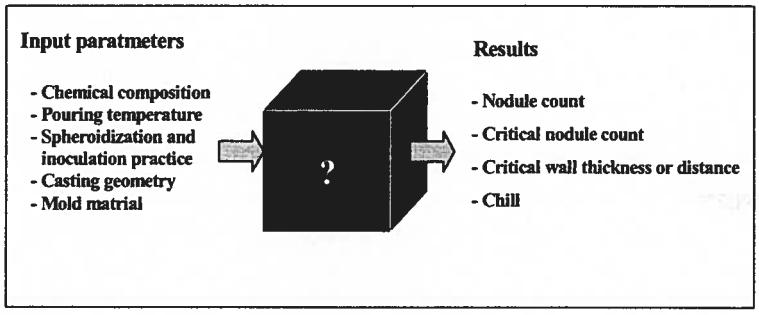

Fig. 1. Black box of possible relationships between various casting input and output parameters

2. Experimental

Experimental melts were obtained in an electric induction furnace with a 15 kg capacity crucible. The raw materials were sorel-metal and commercially pure silicon. The metal was preheated at 1500°C and then poured into the mold which was equipped with a reaction chamber connected to a pouring basin and containing a mixture of 53 g of spheroidizer (Elmag 5800; 44–48% Si, 5.5–6.2% Mg, 0.8–1.2 RE, 1.0% max. Al) and 30 g of inoculant (Foundrysil; 73-78% Si, 0.75–1.25% Ca, 0.75–1.25% Ba, 0.75–1.25% Al). After filling the pouring basin, a graphite plug was removed allowing metal flow into the mold cavity. The chemical composition of cast iron was C = 3.74%; Si = 3.02%; Mn = 0.12%; P = 0.02%; S = 0.01%; Mg = 0.025%. The cast iron was poured into plate shaped mold cavity with wall thickness, s = 0.16 cm and length 20.0 cm (see Fig.2). The thermocouples Pt-PtRh10 were placed in cross-runner in order to determined cooling curve. From cooling curve, temperature T_p = 1280°C of cast iron entered into mold cavity were recorded. Length of obtained samples was shorter than length of mold cavity and amounted about 17.5 cm.

Metallographic evaluations of the nodule count, as well as cementite and ferrite fractions were made on samples cut from the plates. The average nodule count (average number of graphite nodules per unit area), N_F was measured using a Leica QWin quantitative analyzer. Settings for measurements were as follows: magnification 200 x, calibration and detection threshold was set to 1 mm. In ductile iron the graphite nodules are characterized by a Raleigh distribution [24]. In this case the volumetric nodule count N (the average number of graphite nodules per unit volume) can be related to N_F using the Wiencek equation [25]:

$$N = \sqrt{\frac{N_F^3}{f_g}}, \tag{1}$$

where f_g is the volume fraction of graphite, in hypereutectic TWDI cast iron $f_g \approx 0.14$.

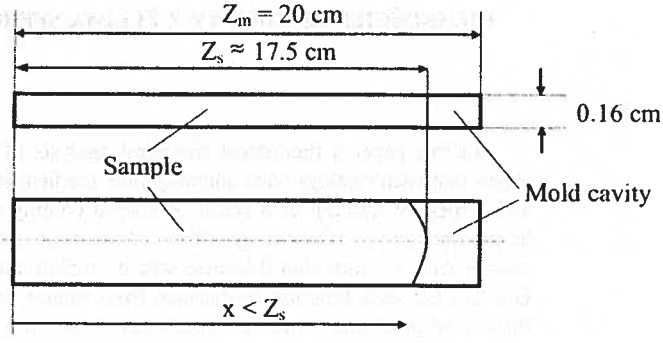

Fig. 2. Shape and size of mold cavity and thin-walled samples

3. Results and analysis

The results of metallographic evaluations are given in Table 1. Experimental results (Fig. 3) are approximated by the following equations:
Graphite nodule count (corelation coefficient R = 0.97)

$$N_F = 2451 + 4.75\ \exp(0.36x) \tag{2}$$

Gradient of Graphite nodule count

$$G_{N_F} = \frac{dN_F}{dx} = 1.71\exp(0.36x). \tag{3}$$

Ferrite fraction (correlation coefficient R = 0.98)

$$f_f = 24.94 - 2.98x + 0.31x^2 - 0.01x^3. \tag{4}$$

Gradient of ferrite fraction

$$G_{f_f} = \frac{df_f}{dx} = -2.98 + 0.62x - 0.03x^2. \tag{5}$$

Cementite fraction (corelation coefficient R = 0.98)

$$f_c = 21.0798x - 341.1. \tag{6}$$

Gradient of cementite fraction

$$G_{f_c} = \frac{df_c}{dx} = 21.08. \tag{7}$$

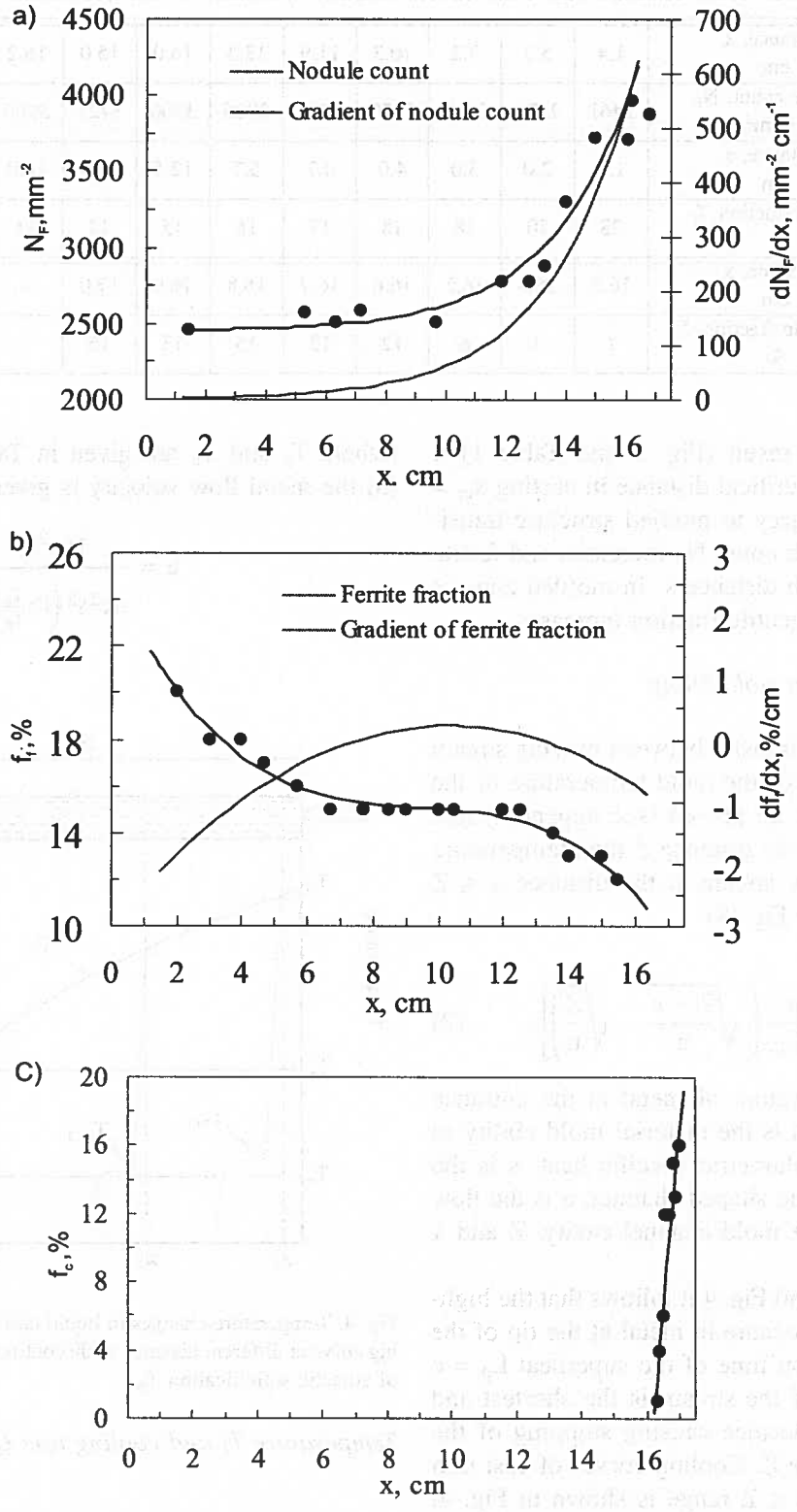

Fig. 3. Influence of distance x on nodule count and gradient of nodle count (a), ferritte fraction and gradient of ferrite fraction (b) and cementite fraction (c) along with regression curves

TABLE 1

Nodule count, cementite and ferrite fraction measured at distance x from cross-runner

Distance, x cm	1.4	5.3	7.2	10.3	11.9	13.3	14.0	15.0	16.2	16.8
Nodule count, N_F $1/mm^2$	2461	2574	2588	2620	2772	2886	3300	3722	3966	3877
Distance, x cm	1.3	2.0	3.0	4.0	4.7	5.7	12.5	13.5	14.0	15.5
Ferrite fraction, f_f %	28	20	18	18	17	16	15	14	13	12
Distance, x cm	16.3	16.4	16.5	16.6	16.7	16.8	16.9	17.0	–	–
Cementite fraction, f_c %	1	4	6	12	12	15	13	16	–	–

From experimental result (Fig. 3 and Table 1) it follows that there exists critical distance in casting x_{cr} = 16.2 cm when there is grey to mottled structure transition. In grey zone nodule count N_F increases and ferrite fraction f_f decreases with distance x. In mottled zone as distance x increases cementite fraction increases.

Temperature drop during mold filling

As a results of heat transfer between moving stream of liquid iron and walls of the mold temperature of the stream decreases. It can be proved (see appendix) that if tip of the stream is at the distance Z then temperature of liquid metal T_i inside stream at the distance $x \leqslant Z$ (Fig. 7) can be given by Eq. (8)

$$T_i = T_p exp\left[\frac{4a}{\sqrt{\pi}cs}\left(\sqrt{\frac{Z-x}{u}} - \sqrt{\frac{Z}{u}}\right)\right], \qquad (8)$$

where: T_p is the temperature of metal at the entrance to the channel (x = 0), a is the material mold ability to absorb heat, c is the volumetric specific heat, s is the wall thickness of the plate shaped channel, u is the flow velocity for metal in the mold channel cavity, Z and x are defined in figure 4.

From equation (8) and Fig. 4 it follows that the highest temperature drop T_i occure in metal at the tip of the stream. Therefore emition time of the superheat $L_p = c(T_i - T_s)$ from the tip of the stream is the shortest and it solidify in the first instance causing stopping of the stream tip at the distance Z. Cooling curves of cast iron for a few points from $x \leqslant Z$ range is shown in Fig. 4. Appropriate for these points cooling curves shows that as distance x decreases temperature of eutectic transformation T_m increases as a result of necessity of carrying away increasing superheat. As it was mentioned before at distance Z tip of the stream stops as a result of the solidification process. As a first approximation it can be assumed that at distance Z, temperature $T_i = (T_s + T_c)/2$ (where T_s and T_e are given in Table 2). and from Eq. (8) the metal flow velocity is given by

$$u = \frac{16a^2Z}{\pi c^2 s^2 \left(\ln\frac{T_s}{T_p}\right)^2}. \qquad (9)$$

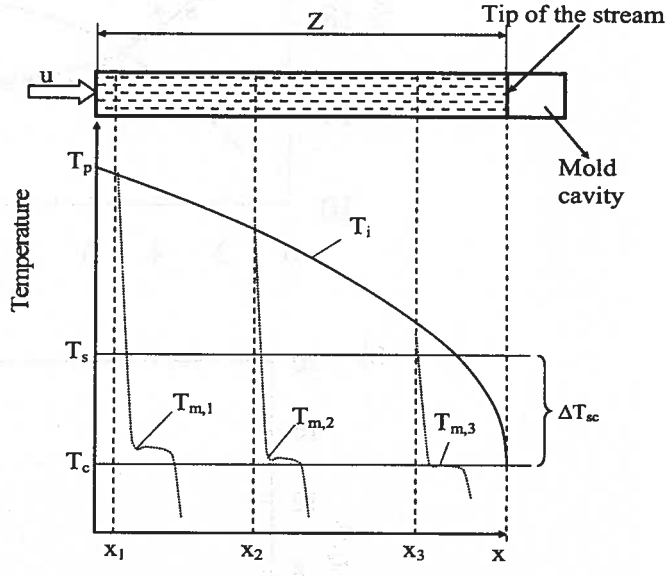

Fig. 4. Temperature changes in liquid cast iron, ΔT_{sc} range and cooling curve at different distance x (discontinuous lines) and temperature of eutectic solidification T_m

Temperature T_i and cooling rate Q

Thin-walled castings are cooled down with high rate and their solidification temperature is close to temperature T_c [26]. The cooling rate of liquid cast iron at a given point of a casting can be given by [27]:

$$Q = \frac{8T_c a^2}{\pi B c^2 s^2}, \qquad (10)$$

where:

$$B = \ln \frac{T_i}{T_c}. \quad (11)$$

From eqs. (8), (10) and (11) it is evident that the cooling rate, among other things also depends on the initial liquid metal temperature, T_i. Figure 5 show cooling rate Q along distance $x \leqslant Z$, calculated according to equations (8)–(11) and using data from table 2. From this figure it follows that as distance x increases coolig rate Q increases especially at the tip of the sample.

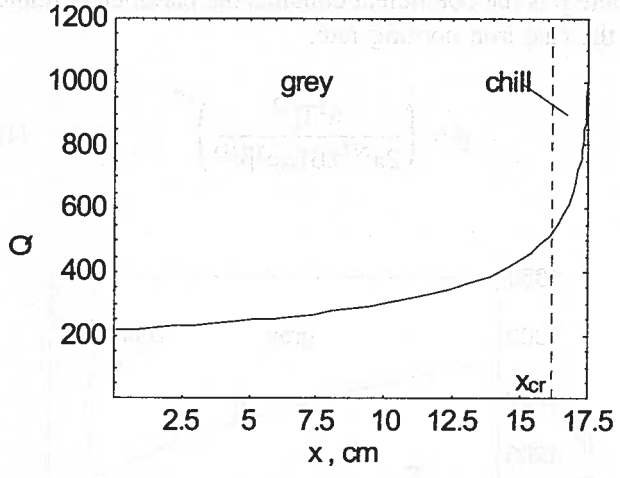

Fig. 5. Influence of distance from runner, x on the cooling rate Q (b) of castings with wall thickness s = 0.16 cm

TABLE 2

Selected thermophysical data

Parameter	Values and units
Material mold ability to absorb heat	a = 0.09–0.11; J/(cm^{2}s$^{1/2}$ °C)
Equilibrium temperature of graphite eutectic	T_s = 1153.9 + 5.25 Si; °C
Solidification temperature of the of cementite eutectic	T_c = 1130 + 4.1(C-3.3 Si); °C
Latent heat of graphite eutectic	L_e = 2028.8; J/cm^3
Diffusion coefficient of carbon in austenite	D = 3.9 × 10^{-6}; cm^2/s
Specific heat of cast iron	c = 5.95; J/(cm^3 °C)
Coefficient related to the slopes of the solubility lines JE', E'S' and BC' in the Fe-C system	β = 0.00155; °C^{-1}
Nucleation coefficients of graphite	N_s = 6.8 10^{10}; cm^{-3} b = 285.4; °C
C, Si – are the carbon and silicon contents in cast iron, respectively.	

Nodule count and gradient of nodule count

A theoretical analysis for the solidification of ductile cast iron [27] indicates that the nodule count N can be related to the maximum undercooling $\Delta T_m = T_s - T_m$, (where T_m is the minimum temperature at the onset of the eutectic solidification) by the equation:

$$N = \frac{c\, B^{1/2}}{4\pi z\, L_e} \left(\frac{Q^3}{2D^3\beta^3 \Delta T_m^4} \right)^{1/2}, \quad (12)$$

where:

$$z = 0.41 + 0.93B. \quad (13)$$

In above equations, c, D, L_e, and β are defined in Table 2.

From Eq. (12), for a given cooling rate, results that Q the nodule count increases as the maximum undercooling ΔT_m decreases what is in agreement with the experimental outcome.

According to the literature [28, 29], a relation between the maximum degree of undercooling ΔT_m and the nodule count N can be described by

$$N = N_s \exp\left(-\frac{b}{\Delta T_m}\right). \quad (14)$$

where N_s and b – are the nucleation coefficients (N_s is the density of nucleation sites for graphite nucleation while b depends on the size of nucleation sites).

From Eqs. (10) and (12) ΔT_m can be calculated, which upon substitution into Eq. (14) yields

$$N = \frac{N_s}{\exp\left[2\,\text{ProductLog}\,(y)\right]}, \quad (15)$$

where:

$$y = \frac{b\, c}{4} \left(\frac{z\, B\, L_e N_s s^3}{a^3} \right)^{1/2} \left(\frac{\pi^5 D^3 \beta^3}{T_c^3} \right)^{1/4}. \quad (16)$$

The Product Log[y] = x is the Lambert function, also known as the omega function and it is graphically shown in Fig. 6. This function can be easily calculated by means of the instruction ProductLog[y] in the Mathematica™ programme.

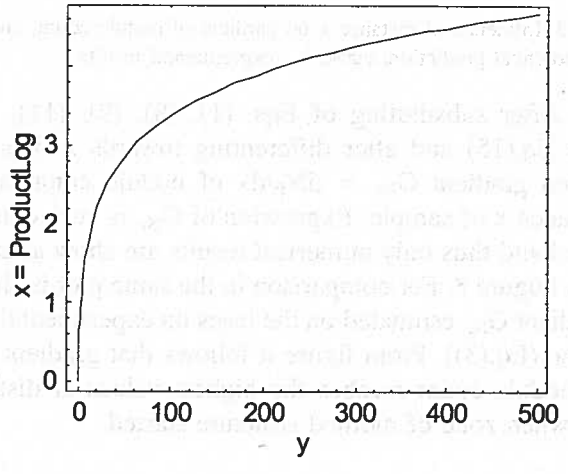

Fig. 6. Function x = ProductLog[y]

Taking into account parameters from Table 2 and by employing Eqs. (1), (8), (9), (11), (15) and (16) very

complicated function of $N_F = f(x)$ can be calculated. Curve in Figure 7 shows plot of this function for data given in table 2. From this figure it can be found that the nodule count increases as the distance x from the runner increases. Notice from this figure rather a good agreement between the theory and the experimental outcome.

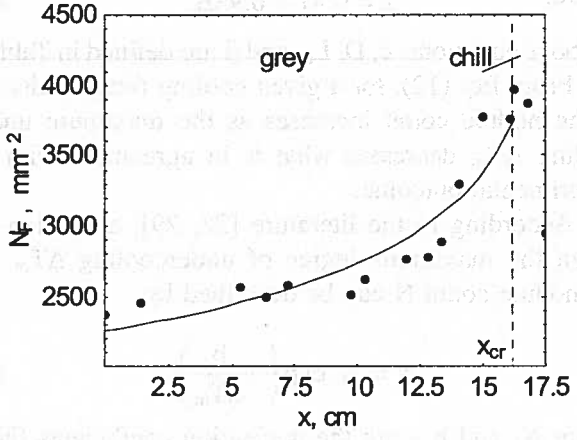

Fig. 7. Influence of distance x on nodule count, points – experimental results, Z = 17.5 cm, x_{cr} = 16.2 cm, T_p = 1280°C

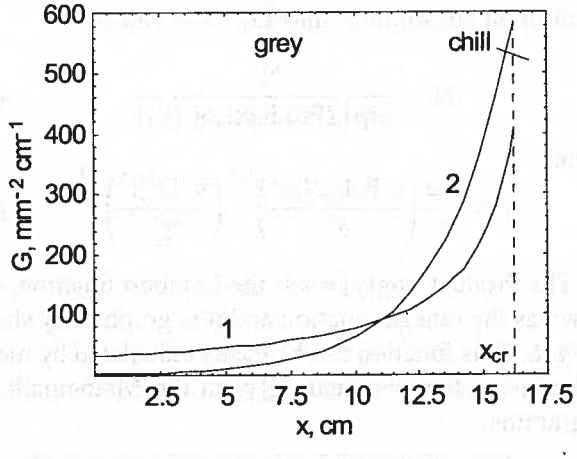

Fig. 8. Influence of distance x on gardient of nodule count, curve 1 – theoretical prediction, curve 2 – experimental results

After substituting of Eqs. (1), (8), (9), (11), (16) into Eq.(15) and after differenting towards x it is obtained gradient $G_{N_F} = dN_F/dx$ of nodule count along distance x of sample. Expression of G_{N_F} is very complicated and thus only numerical results are show as curve 1 in fiugure 8. For comparison in the same plot is shown gradient G_{N_F} estimated on the basis on experimental outcome (Eq.(3)). From figure it follows that gradient G_{N_F} of nodule count reaches the highest values at distance x_{cr} when zone of mottled structure started.

Minimal temperature for graphite eutectic solidification

From Table 1 follows that in sample with 17.5 cm in length (see Fig. 2) cementite eutectic occure (chill) at the distance Z = 16.2 cm. It means that at the distance Z temperature T_m of the solidification of graphite eutectic equals to the solidification of the cementite eutectic T_c while undercooling $\Delta T_m = T_s - T_m$ reaches $\Delta T_{sc} = T_s - T_c$. The minimal temperature T_m for graphite eutectic can be calculated from Eqs. (10) and (12).

$$T_m = T_s - p\left(\frac{64}{N^2\beta^3 D^3 s^6}\right)^{1/4}, \qquad (17)$$

where p is the coefficient contains the parameters related to the cast iron cooling rate,

$$p = \left(\frac{a^3 T_c^{3/2}}{2\pi^{5/2} z B L_e c^2 \beta^{1/2}}\right)^{1/2}. \qquad (18)$$

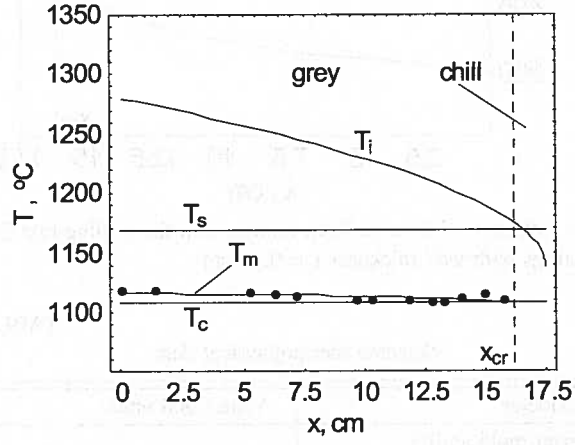

Fig. 9. Influence of distance from runner, x on the temperatures Ti and T_m of casting with wall thickness s = 1.6 mm

Taking into account experimental results of N_F (Table 1) and data from Table 2 as well as equations (1), (8), (9), (17) and (18) the minimal temperature, T_m for graphite eutectic solidification as a function of distance, x can be calculated. Results of these calculations by means of points are shown in figure 9. After substituting Eq. (14) into Eq. (17) and its solving it is obtained

$$T_m = T_s - \frac{b}{2\text{ProductLog}[y]}. \qquad (19)$$

Equation (19) enables to calculate T_m knowing nucleation parameters N_s and b. Results of such calculation after taking into consideration Eqs. (1), (8), (9) and (19) and data from Table 2 is shown as a solid line in Fig. 9. Notice that differences in results between calculated nodule count and using nucleation coefficients N_s and b are rather small.

Chilling tendency and critical distance x_{cr}

It is well known, that as $T_m = T_c$ or $\Delta T_m = T_s - T_c = \Delta T_{sc}$ the cementite eutectic begins to solidify. By taking into account this condition and Eqs. (8), (11), (13), (17) and (18) it can be obtained

$$x_{cr} = \frac{1}{8a^2} c\sqrt{\pi} us \left[A - \ln\left(\frac{T_c}{T_p}\right)\right] \left[4a\sqrt{\frac{Z}{u}} + \frac{1}{2} c\sqrt{\pi} s\left(\ln\left(\frac{T_c}{T_p}\right) - A\right)\right], \quad (20)$$

where

$$A = 0.22 - 0.54\sqrt{0.17 + \frac{0.85a^3 T_c^{3/2}}{c^2 L_e s^3 \beta^{1/2}} CT^3}. \quad (21)$$

CT is chilling tendency, given by

$$CT = \left(\frac{1}{N_s^2 \beta^2 D^3 \Delta T_{sc}^4}\right)^{1/6} \exp\left(\frac{b}{3\Delta T_{sc}}\right) \quad (22)$$

or knowing the critical nodule count (critical nuclei density) N_{cr} at temperature T_c

$$CT = \left(\frac{1}{N_{cr}^2 \beta^2 D^3 \Delta T_{sc}^4}\right)^{1/6}. \quad (23)$$

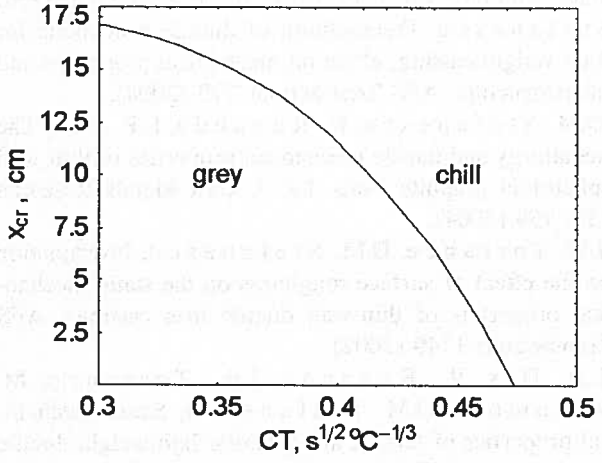

Fig. 10. Influence of chilling tendency CT on critical length x_{cr} of casting above which chills occure in casting

On the basis on equations (20)–(23) the critical distance x_{cr} above which a chill is likely to form can be calculated. Chilling tendency which is calculated according to Eq. (22) for data taken from Table 2, amounts CT = 0.34 $s^{1/2}/°C^{1/3}$, while critical length of a sample x_{cr} = 15.90 cm (Eqs. (8), (9), (11), (20) and (21)). From Table 1 it follows that at the critical nodule cont N_F = 3966 mm^{-2} chills occure in sample. After recalculation N_F into N (Eq.(1)) for data from Tabeli 2, according to equations (21), (22) and (23) it is obtained CT = 0.32 $s^{1/2}/°C^{1/3}$ and critical length of sample x_{cr} = 16.4 cm. It is worth mentioning that both calculated values of x_{cr}, are close to an experimental value x_{cr} = 16.2 cm. In foundry practice inoculation process strongly decreases chilling tendency CT. Calculated influence of CT on critical sample length x_{cr} is shown in figure 10 from it is seen that as CT increases also increases chilled zone up to 17.5 cm

4. Concluding remarks

1. It has been shown that despite of the constant wall thickness, the microstructural features of TWDI can be inhomogeneous (nodule count, chill, ferrite fraction) along its length as a result of changes in the cooling rates.
2. From the proposed theory new expressions are derived for the critical distanece x_{cr} and gradient of nodule count G_{N_F} for ductile cast iron.
3. Theoretical calculations for the critical distanece x_{cr} and nodule count were made and compared with the experimental outcome and rather a good agreement was found between the theoretical predictions and the experimental outcome.

5. Appendix

It is assumed (see Fig. 11) that liquid metal flows through a molding sand channel of constant cross section at constant velocity, u. At the stream front where x = Z, the convective heat transfer coefficient α is relatively large due to contact of the metal stream with the cold mold, while at the chanell entrance (x = 0, warm mold) is small. Under these conditions, heat transfer occurs normal to the metal flow direction. The convective heat transfer coefficient can be described by [30]:

$$\alpha = \frac{a}{\sqrt{\pi\left(\frac{Z-x}{u}\right)}}. \quad (A1)$$

From heat balance equation results:

$$dQ_m = dQ_a, \quad (A2)$$

where Q_m, and Q_a are the heat going towards the mold, and the heat accumulated in the metal, respectively. Considering a volume element of liquid metal, V, the heat dissipated, dQ_m can be described by

$$dQ_m = \alpha T_i F dt, \quad (A3)$$

where F is the surface area of liquid metal in contact with the mold channel, T_i is the temperature of metal at any location x away from the entrance.

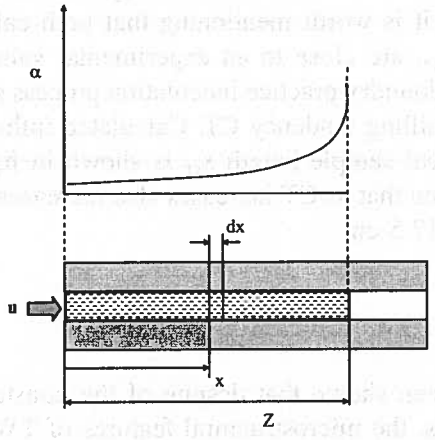

Fig. 11. Stream of liquid cast iron in molding channel and change of convective heat transfer coefficient α into molding material

Moreover, dQ_a can be described by

$$dQ_a = -VcdT_i, \tag{A4}$$

where c is the metal heat capacity. Considering constant u, that is dt = dx/u a comparison between Eqs. (A3) and (A4) yields after integration

$$\ln T_i = \frac{2aF}{c\sqrt{\pi V}}\sqrt{\frac{Z-x}{u}} + C. \tag{A5}$$

In the above expression, C can be found from the condition: at x = 0, (at the entrance to the chanell), the liquid metal temperature $T_i = T_p$, thus:

$$\ln T_p - \frac{2aF}{c\sqrt{\pi V}}\sqrt{\frac{Z}{u}} = C. \tag{A6}$$

Substituting Eq. (A6) into Eq. (A5) and taking into account the liquid metal modulus M = V/F ≈ s/2, where s is the wall thickness of the plate shaped channel, the temperature of the metal can be described by:

$$T_i = T_p \exp\left[\frac{4a}{\sqrt{\pi}cs}\left(\sqrt{\frac{Z-x}{u}} - \sqrt{\frac{Z}{u}}\right)\right]. \tag{A6}$$

Acknowledgements

This work was supported by Grant KBN-3T08B04230, and the work was made in the Department of Cast Iron at AGH University of Science and Technology, Cracow, Poland.

REFERENCES

[1] M. Koizumi, Recent Progress of Functionaly Gradient Materials in Japan, Ceramic Engineering and Science Proceedings **14**, 333 (1992).
[2] K.L. Choy, Functionaly Graded Materials, The Encyklopedia of Advanced Materials, Pergamon, Cambridge Univerity Press, Elsevier Scence Ltd., (1994).
[3] R. Pampuch, Materiały ceramiczne-zarys nauki o materiałach nieorganiczno-niemetalicznych, PWN, Warszawa (1988).
[4] K.K. Schrems, O.M. Dogan, J.A. Hawk, Verification of thin-wall ductile iron test, ASTM International **47**, (2002).
[5] D.M. Stefanescu, R. Ruxanda, L.P. Dix, The metallurgy and tensile mechanical properties of thin wall spheroidal graphite irons, Int. J. Cast Metals Research **117**, 759 (2004).
[6] C.E. Yeung, H. Zhao, W.B. Lee, The morphology of solidification of thin-section ductile iron castings, Materials characterization, Elsevier Science Inc. (1998).
[7] R.E. Ruxanda, D.M. Stefanescu, T.S Piwonka, Microstructure characterization of ductile thin wall iron castings, AFS Transactions 1131 (2002).
[8] O.N. Dogan, K.K. Schrems, J.A. Hawk, Microstructure of thin wall ductile iron castings, AFS Transactions 949 (2003).
[9] D.M. Stefanescu, L.P. Dix, R.E. Ruxasnda, C. Corbitt-Coburn, T.S. Piwonka, Tensile properties of thin wall ductile iron, AFS Transactions 1149 (2002).
[10] F.R. Juretzko, L.P. Dix, R. Ruxanda, D.M. Stefanescu, Precondition of ductile iron melts for light weight casting; effect on mechanical properties and microstructure, AFS Transactions 773 (2004).
[11] D.M. Stefanescu, R. Ruxanda, L.P. Dix, The metallurgy and tensile mechanical properties of thin wall spheroidal graphite irons, Int. J. Cast Metals Research **117**, 759 (2004).
[12] J.W. Torrance, D.M. Stefanescu, Investigation on the effect of surface roughness on the static mechanical properties of thin-wall ductile iron castings, AFS Transactions 1149 (2002).
[13] L.P. Dix, R. Ruxanda, J.W. Torrance, M. Fukumoto, D.M. Stefanescu, Static mechanical properties of ferritic and pearlitic lightweight ductile iron castings, AFS Transactions 895 (2003).
[14] A. Javaid, J. Thomson, K.G. Davis, M. Sahoo, Effect of microstructure on the mechanical properties of thin-wall ductile iron castings, AFS Transactions 1097 (2001).
[15] A Javaid, J. Thompson, M. Sahoo, K.G. Davis, Factors Affecting the Formation of Carbides in Thin-wall DI Castings, AFS Transactions 441 (1999).
[16] A. Javaid, M. Thompson, K.G. Davis, Critical conditions for obtaining carbide – free microstructure in Thin-Wall Ductile irons, AFS Transactions 889 (2002).

[17] C. Labrecque, M. Gagne, Production of thin-wall ductile iron castings, Int. J. Cast Metals Research **16**, 313 (2003).

[18] J.F. Cuttino, J.R. Andrews, T.S. Piwonka, Development in thin-wall iron casting technology, AFS Transactions 363 (1999).

[19] J.M. Massone, R.E. Boeri, J.A. Sikora, Solid state transformation kinetics of high nodule count ductile iron, Int. J. Cast Metals Research **16**, 179 (2003).

[20] A. Giacopini, R.E. Boeri, J.A. Sikora, Carbide dissolution in thin wall ductile iron, Mats Sci and Tech **19**, 1755 (2003).

[21] F. Mampaey, Z.A. X, Mold filling and solidification of a thin-wall ductile iron casting, AFS Transactions 95 (1997).

[22] J.H. Choi, J.K. Oh, C.O. Choi, J.K. Kim, P.K. Rohatgi, Effect of Bi Formation of Microstructure and Mechanical Properties of Ductile Iron Castings With Thin-Wall Section, AFS Transactions 831 (2004).

[23] R.E. Showman, R.C. Aufderheide, A Process for Thin-Wall Sand Castings, AFS Transactions 567 (2003).

[24] L. Wojnar, Effect of graphite size and distribution on fracture and fractography of ferritic nodular cast iron, Acta Stereologica **5/2**, 319 (1986).

[25] K. Wiencek, J. Ryś, The estimation of Fe_3C particle density in steel by simple counting measurements made in plan sections, Materialas Engineering **3**, 396 (1998).

[26] K.M. Pedersen, N. Tiedje, Solidification of hypereutectic thin wall ductile iron, Materials Science Forum **508**, 64-68 (2006).

[27] E. Fraś, M. Górny, H.F. López, Eutectic Transformation in Ductile Cast Iron Part I-Theoretical Background, Metallurgy and Foundry Engineering **31**, 113 (2005).

[28] E. Fraś, M. Górny, H.F. López, A dependency between undercooling and eutectic grain density in nodular cast iron – modeling research and their experimental verification, Archives of Metallurgy and Materials **49**, 93 (2004).

[29] E. Fraś, K. Wiencek, M. Górny, H.F. López, Nodule count in ductile iron: theoretical model based on Weibull statistics, Int. J. Cast Metals Research **18**, 156 (2005).

[30] W. Longa, Krzepnięcie odlewów w formach piaskowych, Śląsk (1972).

Received: 10 February 2006.